# NEURAL NETWORK MODELS FOR NON-INVASIVE TWO-POINT TEMPERATURE MONITORING IN A HOMOGENEOUS MEDIUM IRRADIATED BY THERAPEUTIC ULTRASOUND

C. A. Teixeira*, W. C. A. Pereira**, A. E. Ruano*, C. Negreira*** and M. Graça Ruano*

* Centro de Sistemas Inteligentes/Faculdade de Ciências e Tecnologia, Universidade do Algarve, Faro, Portugal
** Programa em Engenharia Biomédica/COPPE, Universidade Federal do Rio de Janeiro, Rio de Janeiro, Brasil
***Laboratorio de Acústica Ultrasonora, Facultad de Ciencias, Universidad de la República, Montevideo, Uruguay

cateixeira@ualg.pt

**Abstract: In this paper the performance of neural network models for non-invasive temperature prediction in two points of a glycerine medium, irradiated with therapeutic ultrasound is investigated. These points are located in the axial line of the therapeutic ultrasound transducer. It is assumed that the temperature in these points is non-linearly related with some spectral features and one temporal feature, extracted from the collected A-Scans. The neural networks used were Radial Basis Functions Neural Networks (RBFNN), where the best-fitted models structures for each point were selected in a genetic multi-objective fashion, due to the enormous number of possible model structures. The best-fitted models predicted temperature curves of two unseen data sequences during approximately 2 hours with maximum absolute errors less than 0.5 ºC.**

## Introduction

One of the major limitations of thermal therapies is the lack of accurate knowledge of the temperature patterns in the region under treatment. Precise temperature predictors (absolute error less than 0.5 ºC [1]) would enable correct therapy guidance, by means of an efficient Therapeutic Ultrasound (TUS) instrumentation control. Many works describing ways of estimating temperature non-invasively have been published. Possible methods include impedance tomography, microwave radiometry, and magnetic resonance imaging. Some works employ ultrasonic conventional imaging to estimate the temperature in time and space. The work of Simon et al. [2] uses Imaging UltraSound (IUS) thermometry and considers temperature linearly related with sound velocity and medium expansion. It achieves a maximum absolute error of 0.44 ºC, an average error of –0.02 ºC, and a mean squared error of 0.03 $(ºC)^2$ at the focus of the TUS transducer, where the temperature ranged between 20.5 ºC and 24.5 ºC in 90 seconds.

The present work evaluates the potential of a non-linear Neural Network (NN) model for non-invasive estimation of the temperature profile at two discrete points, in a glycerine reservoir irradiated with physiotherapeutic ultrasound. These points are 24 and 48 mm distant from the TUS transducer face. This work follows previous studies in punctual and invasive temperature estimation using a similar modelling strategy. The results obtained showed that these models performed well in this kind of problems [3].

Manual selection of the best-fitted NN structures is a high time consuming task given the enormous number of possible structures. In this work, the Multi-Objective Genetic Algorithm (MOGA) [4] was applied to handle this problem. The MOGA was applied with success in other problems involving RBFNN structure selection [3][5], encouraging its use in the present work.

## Materials and Methods

A circular shape TUS transducer working at 1 MHz, with a nominal effective radiation area of 3.5 $cm^2$ irradiates continuously a 1400-ml glycerine reservoir, containing an irregular-shaped surface material at the bottom and walls to prevent standing waves formation. In order to obtain acoustic information from the two points considered, three scatterers (3-mm-radius lead spheres) were placed in a plan parallel to the TUS transducer face. The scatterers were 1-cm spaced and the central one was 24 or 48 mm distant from the TUS transducer face. A cromel-alumel (Type K) thermocouple was placed near to the central sphere. To perform non-invasive temperature estimates A-Scans (AS) were collected with a 5-MHz non-focused IUS transducer driven by a PC controlled pulser/receiver. The IUS beam insonates the scatterers in a plan perpendicular to the TUS beam. At each 10 seconds, during a 2-hour experiment time, an AS (2048 points, sampled at 40 MHz) line was saved, with its correspondent temperature value. For each scatterer distance, three sets of data were collected, corresponding to TUS intensities of 1.0, 1.5 and 2.0


ISSN: 1727-1983 © 2005 IFMBE

W/cm$^2$. The correspondent temperature ranges obtained are shown in Table 1.

Table 1: Temperature ranges

| Distance (mm) | Intensity (W/cm$^2$) | Temperature (ºC) Initial | Max. | Final |
|---|---|---|---|---|
| 24 | 1.0 | 29.6 | 35.7 | 29.7 |
| | 1.5 | 29.9 | 37.8 | 30.7 |
| | 2.0 | 24.6 | 34.7 | 29.8 |
| 48 | 1.0 | 28.3 | 33.1 | 29.2 |
| | 1.5 | 24.5 | 34.8 | 28.3 |
| | 2.0 | 28.2 | 38.2 | 31.2 |

For each set, a total of 720 temperature points and corresponding AS were obtained. The glycerine was heated during the first hour. Then the TUS beam was interrupted and the medium left to cool back to room temperature. Figure 1 presents the schematic diagram of the experimental setup.

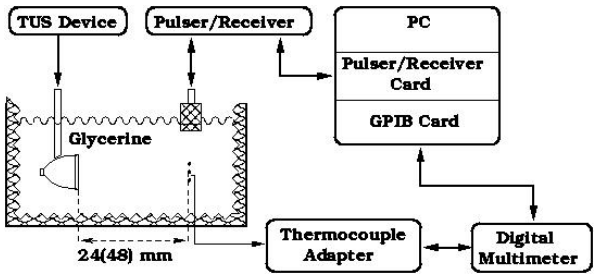


Figure 1: Experimental setup.

The construction of RBFNN models for temperature monitoring required temperature-dependent features, extracted from the collected AS. Given that temperature collection was only made in the central scatterer, for the two distances, features extraction was only performed in the echo originated by this scatterer in conjunction with the thermocouple, in order to discard information originated by other scatterers placed in regions subjected to different TUS beam patterns, and where the temperature profile was different from the testing point. A rectangular time-window was used to isolate the echo, then a Fast Fourier Transform was applied, and six spectral features computed. These features where: the amplitude of the fundamental component originated by the TUS beam (≅ 1 MHz), the amplitude of the 1st (≅ 2 MHz) and 2nd (≅ 3 MHz) harmonics of the fundamental component originated by the TUS beam, and amplitude, bandwidth (-6 dB), and central frequency of the component originated by the IUS beam (≅ 5.5 MHz). The only temporal feature extracted was the time position of the envelope echo originated by the central scatterer. The envelope was obtained by the Hilbert transform procedure.

Afterwards, the features extracted and the measured temperature values were filtered using a causal Butterworth digital filter (cut-off frequency = 1/20 of the Nyquist frequency; order=1), and normalised to values between 0 and 1. The filter parameters were selected having in mind the noise reduction present in the extracted features, preserving its fundamental behaviour. The normalisation was necessary to eliminate the scale differences that could lead to a bad NN training. For the remaining of this paper, the following conventions are used:

- Normalised and filtered amplitude of the fundamental component originated by the TUS beam - $\mathbf{AF_{TUS}}$;
- Normalised and filtered amplitude of the 1st and 2nd harmonics of the fundamental component originated by the TUS beam - $\mathbf{AH1_{TUS}}$ and $\mathbf{AH2_{TUS}}$;
- Normalised and filtered amplitude, bandwidth, and central frequency of the component originated by the IUS beam – $\mathbf{A_{IUS}}$, $\mathbf{BW_{IUS}}$, and $\mathbf{F_{IUS}}$;
- Normalised and filtered temporal position – **TP**;
- Normalised and filtered temperature – **T**.

At the end of this pre-processing phase, the parameters optimisation of the RBFNN (training) was obtained using random data selected from the three measured sets (1/3 from each set), for each distance, i.e., two training sets were obtained having in mind the attainment of two class of RBFNN, one for each point considered (24 mm and 48 mm). In the structure selection process the MOGA access the generalisation performance (i.e. performance in unseen data sequences) of the RBFNN candidates, using the data collected at 1.5 W/cm$^2$. At the end of the MOGA execution two sets of best-fitted RBFNN were found and the selection of the two best one was based on the performance attained in two validation data sequences (not yet used in training or selection processes), collected at 2 W/cm$^2$. The motivation for choosing data from 2 W/cm$^2$ was the fact that these data presented more non-linearities than the other sets of data.

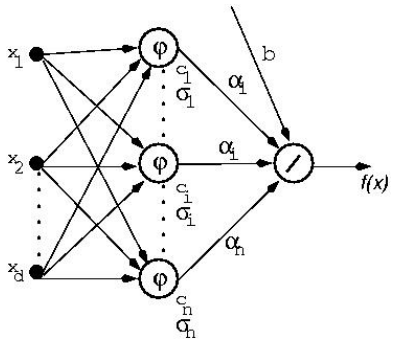


Figure 2: Schematic diagram of a RBFNN.

A RBFNN is a fully connected three-layer NN (Fig. 2) where the first layer is a set of inputs, which connects the network to its environment. The second layer, the only hidden layer in the NN, is composed by a set of processing elements called neurons, which performs a non-linear transformation on the input data. The outputs of the hidden layer are linearly combined and connected


ISSN: 1727-1983 © 2005 IFMBE

to the last layer to produce the overall NN output. The input/output relation for a RBFNN is:

$$f(x_j) = b + \sum_{i=1}^{n} \alpha_i \varphi\left(\left\| x_j - c_i \right\|\right) \qquad (1)$$

where *n* is the number of neurons in the hidden layer, *b* is the bias term, ||.|| is a norm, in this particular work an Eucledian norm was used, and $\{\varphi(.)\}_{i=1}^{n}$ is a set of non-linear radial basis functions weighted by $\{\alpha_i\}_{i=1}^{n}$ and centred at $\{c_i \in \Re^d\}_{i=1}^{n}$, being *d* the number of inputs. These functions are evaluated at points $x_j \in \Re^d$ and are usually represented by Gaussian functions:

$$\varphi_i = e^{\frac{1}{2\sigma_i^2}\left\| x_j - c_i \right\|^2} \qquad (2)$$

In this work, the MOGA structure optimisation consists in the appropriate selection of the number of neurons in the hidden layer and the selection of inputs by their relevance on the model. The possible input candidates are the lags of $AF_{TUS}$, $AH1_{TUS}$, $AH2_{TUS}$, $A_{IUS}$, $BW_{IUS}$, $F_{IUS}$, TP, and T. In our work, the MOGA spams 200 iterations (generations), of 100 RBFNN (individuals) each. The crossover and mutation probabilities were set to be 0.7 and 0.5, respectively. To maintain population diversity, 10 % of the old population was changed, in each iteration, by a set of randomly generated RBFNN (corresponding to 10 RBFNN). These MOGA parameters are the ones that produce the best results for this specific problem, and were selected after performing several tests. The MOGA search space was bounded by defining the possible number of neurons and inputs, and the maximum admissible lag for the input variables. Both the number of neurons and the number of inputs were defined to be integers in the interval [2,20], and the Maximum LAG (MLAG) was defined as 20. This means that the MOGA can choose models, which can use information happened up to 200 seconds in the past. These values are also selected after several tests considering other possibilities. Assuming the number of input variables NV=8, the total number of input terms that were available was $IT = MLAG \times NV = 160$, then the total number of inputs combinations (*NIC*) is given by:

$$NIC = \sum_{n=2}^{20} {}^{IT}C_n = 1.7E25 \qquad (3)$$

Considering the restriction in the number of neurons, then the total number of possible RBFNN structures (*TNS*) is:

$$TNS = 20 \times NIC = 3.3E26 \qquad (4)$$

This number justifies the application of a genetic selection instead of an exhaustive "manual" selection.

The training of each individual was performed using the Levenberg-Marquardt (LM) algorithm, which is recognised as the best method for non-linear least-squares problems [6], which is the case of RBFNN training. The LM optimises only the values of the centres ($\{c_i\}_{i=1}^{n}$) and spreads ($\{\sigma_i\}_{i=1}^{n}$), while the linear parameters (*b* and $\{\alpha_i\}_{i=1}^{n}$) were found using the linear least squares strategy. The initial value of the centres and spreads were found using the Optimal Adaptive K-Means clustering algorithm [7], and the "early-stopping" criterion was used to terminate the parameters optimisation. This termination criterion access the performance of the NN in the test data sequence (in this case the data collected at 1.5 W/cm$^2$) and the LM stops when this performance deteriorates, preventing model over-training (i.e. NN which models the noise and are only specialised in the training data).

In each MOGA iteration, after training, the performance of each individual was accessed and it's ranking was executed. In the ranking operation, the NNs are sorted to improve the selection and reproduction of the best fitted. The performance was evaluated according to the following measures:

- Root Mean Square Error in the Training set ($RMSE_{TR}$);
- Root Mean Square Error in the Test set ($RMSE_{TE}$). This error is obtained by predicting the temperature 1 step ahead;
- Maximum Root Mean Square Error in all the Prediction Steps ($MRMSE_{PS}$). This error is obtained by predicting the temperature 60 steps in the future, using the test sequence, and taking the maximum error obtained in all the predictions steps;
- Model-validity tests;
- Linear Weights Norm (LWN);
- Model Complexity (MC).

The model-validity tests are explained in [8], and used in [5]. These tests involve the computation of the first and higher order correlations between model inputs, errors, and outputs. As explained in [8], if a model is adequate then a set of 8 conditions should hold. In the work reported in this paper only the conditions involving the first order correlations were used, because the results obtained using the high order correlations were not better than those presented, thus, not justified its use. The conditions employed were:

$$R_{ee}(\tau) = \delta(\tau) \quad \text{Auto-correlation of the errors} \qquad (5)$$

$$R_{ue}(\tau) = 0 \quad \text{Correlation between inputs and errors} \qquad (6)$$

In fact, $R_{ue}$ will never be exactly zero for all lags, so the equality is considered true if its normalised value is in between a 95% confidence interval defined as:

$$CI = 1.96/\sqrt{N}, \qquad (7)$$

where *N* is the number of training points. In the same way, the value of $R_{ee}$ never equals the delta function, but the equality (5) is considered true if its normalised value is less than *CI* before lag one.


ISSN: 1727-1983 © 2005 IFMBE

The MC was computed as the total number of parameters for a particular NN structure:

$$MC = NC \times NI + NS + NW \text{ ,} \qquad (8)$$

Where *NC* is the number of centres, *NI* is the number of inputs, *NS* is the number of spreads, and *NW=n* is the number of linear weights.

The attainment of best-fitted models encompasses the minimization of the previously referred measures by means of the MOGA. Having in mind the attainment of models with a high generalisation capacity, the $RMSE_{TE}$ and $MRMSE_{PS}$ were defined as goals of priority 2, with values of 0.002 and 0.003, respectively. The maximum of the two correlation tests was defined with a goal value of *CI*=0.074, and with priority 1. In order to attain generalist models, i.e. models that are not only specialised on the training set, the LWN was defined as a goal of value 2 and priority 1. Large models of heavy computation are undesired if its implementation on a real time schema is wished. For this reason MC was defined with a goal value of 100 and priority 1.

**Results**

The MOGA run applied to the signals collected at 24 mm yielded a set of 28 best-fitted individuals (RBFNN), known as Preferable Individuals (PIs). As said before the choice of the best model from the PIs set was based on the performance attained in an unseen data sequence, collected at 2 W/cm$^2$, hereby referred as validation data sequence. In Figure 3, the Maximum absolute Predictive Error (MPE) in this data sequence is presented.

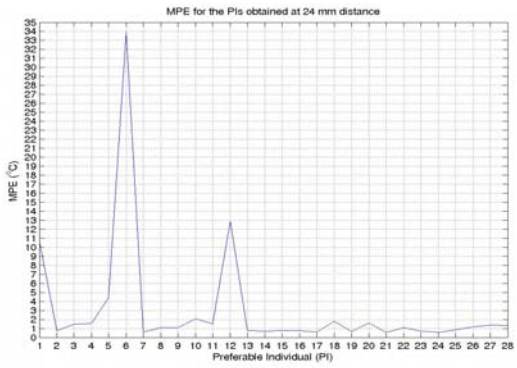


Figure 3: MPE for the PIs at 24 mm distance.

Observing the values of MPE's depicted in this Figure the best PI is the 24, which presents a MPE of 0.49 ºC, an average error of 0.04 ºC and a mean squared error of 0.013 (ºC)$^2$. This model has 11 neurons in the hidden layer and its inputs are listed in Table 2.

Table 2: Inputs of the best PI at 24 mm distance

| | | | Lags of | | | | |
|---|---|---|---|---|---|---|---|
| $AF_{TUS}$ | $AH1_{TUS}$ | $AH2_{TUS}$ | $A_{IUS}$ | $F_{IUS}$ | $BW_{IUS}$ | TP | T |
| 4 | 3 | 3 | 0 | - | 3 | 1 | 4 |
| 17 | | | 17 | | 6 | | 16 |
| | | | | | 19 | | 17 |

The MOGA optimisation objectives for that individual are presented in Table 3.

The performance of the best individual during the validation phase is presented in Figure 4.

Table 3: MOGA results for the best individual at 24 mm.

| | $RMSE_{TR}$ | $RMSE_{TE}$ | $MRMSE_{PS}$ | LWN | MC | $R_{ee}$ | $R_{ue}$ |
|---|---|---|---|---|---|---|---|
| | 0.0016 | 0.0019 | 0.0027 | 1.08 | 166 | 0.0602 | 0.0929 |
| **G** | - | 0.002 | 0.003 | 2 | 100 | 0.0741 | 0.0741 |
| **P** | - | 2 | 2 | 1 | 1 | 1 | 1 |

**G** – MOGA Goals **P** - MOGA Priorities

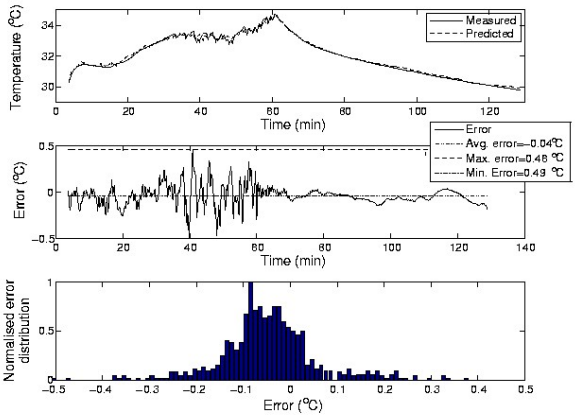


Figure 4: Predicted and measured temperature waveforms in conjunction with the associated error and error distribution, for the best PI at 24 mm distance.

For the 48 mm experiment, the correspondent MOGA run yielded a set of 9 PIs. The MPEs obtained in the validation sequence for this distance are presented in Figure 5. It can be seen that the best PI is the 1, which presents a MPE of 0.38 ºC, an average error of 0.0072 ºC, and a mean squared error of 0.0071 (ºC)$^2$. This model contains 12 neurons in the hidden layer and its inputs are listed in Table 4.

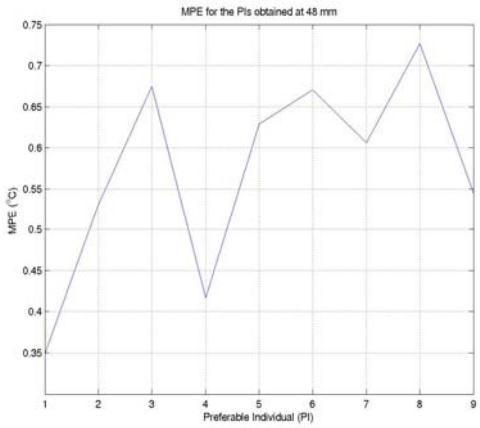


Figure 5: MPE for the PIs at 48 mm distance.


ISSN: 1727-1983 © 2005 IFMBE

Table 4: Inputs of the best PI at 48 mm distance.

| | | | Lags of | | | | |
|---|---|---|---|---|---|---|---|
| $AF_{TUS}$ | $AH1_{TUS}$ | $AH2_{TUS}$ | $A_{IUS}$ | $F_{IUS}$ | $BW_{IUS}$ | TP | T |
| - | 1 | - | 11 | 1 | 8 | 4 | 10 |
| | | | 12 | 6 | | 13 | 15 |
| | | | 14 | | | | 17 |

The MOGA optimisation objectives for that individual are presented in Table 5.

Table 5: MOGA results for the best individual at 48 mm.

| | $RMSE_{TR}$ | $RMSE_{TE}$ | $MRMSE_{PS}$ | LWN | MC | $R_{ee}$ | $R_{ue}$ |
|---|---|---|---|---|---|---|---|
| | 0.0011 | 0.0010 | 0.0013 | 1.59 | 169 | 0.0701 | 0.0687 |
| **G** | - | 0.002 | 0.003 | 2 | 100 | 0.0741 | 0.0741 |
| **P** | - | 2 | 2 | 1 | 1 | 1 | 1 |

**G** – MOGA Goals **P** - MOGA Priorities

The performance of the best individual at 48 mm in the validation phase is presented in Figure 6.

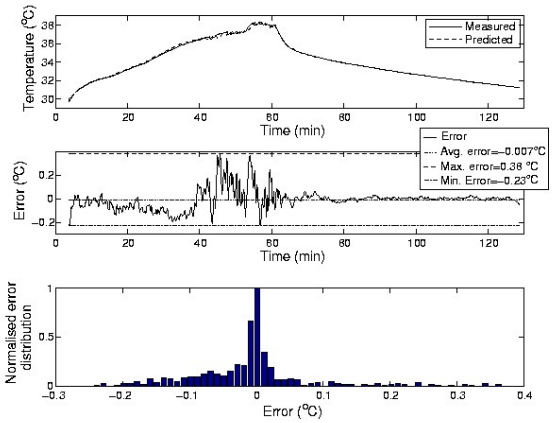


Figure 6: Predicted and measured temperature waveforms in conjunction with the associated error and error distribution for the 48 mm experiment.

**Discussion**

The MOGA applied to the data collected at 48 mm yields only 9 PIs, which have all a MPE inferior to 1 ºC, and two of them have a MPE inferior to 0.5 ºC. On the other hand, for the data collected at 24 mm MOGA returns 28 PIs, and 14 have MPE inferior to 1 ºC. The only one model that presents a MPE inferior to 0.5 ºC is the best-fitted model obtained for this distance. There are also PIs that present an exacerbated error, showing its bad generalisation capacity.

In terms of the number of neurons, the MOGA applied to the 24-mm experiment yielded a best model with 11 neurons, while the 48 mm run yielded a best model with 12 neurons. For both runs, the PI presenting MPEs lower than 1 ºC attained a number of neurons less than 16, demonstrating that temperature modelling for the applied MOGA parameterisation, and for the experimental setup used, would be well performed if the RBFNN had a number of neurons less than 16.

The best PI for the 24-mm experiment has 13 inputs. The relevance of $AF_{TUS}$ for temperature in the conditions of this experiment is represented by the presence of 2 lags ($AF_{TUS}$(k-4) and $AF_{TUS}$(k-17)). The importance of $AH1_{TUS}$ and $AH2_{TUS}$ is marked by the presence of lag 3 of this variables ($AH1_{TUS}$(k-3) and $AH2_{TUS}$(k-3)), i.e. for this parameter arrangement, the valuable information of these variables is the one which is 30 seconds in the past. $A_{IUS}$ relevance is marked by the presence of 2 lags ($A_{IUS}$(k) and $A_{IUS}$(k-17)). In the best individual for the 24-mm experiment, the information of $F_{IUS}$ was completely discarded. This fact does not imply that the information of this variable do not matters for temperature modelling in the present conditions, it only indicates that, for this input arrangement, temperature prediction is well achieved using information from other variables, because in other PI the information of this variable appears as inputs. The importance of the bandwidth information in the best individual input set is represented by 3 lags ($BW_{IUS}$(k-3), $BW_{IUS}$(k-6), and $BW_{IUS}$(k-19)). The temporal position information is marked by the presence of TP(k-1). The past memory of the system is represented by the presence of 3 lags of T (T(k-4), T(k-16) and T(k-17)), demonstrating that T(k) is dependent on the temperature in the past 40, 160 and 170 seconds.

The best PI for the 48-mm experiment has 12 inputs. In this MOGA run the information of $AF_{TUS}$, and $AH1_{TUS}$ was completely discarded from the best individual input set. One more time, this fact does not mean that its information is not important for temperature prediction under present conditions, it just means that, for this input arrangement it is not important, once for other PIs its information appears as inputs. The relevance of $AH1_{TUS}$ is marked by the presence of one lag ($AH1_{TUS}$(k-1)) in the best individual input set, being discarded in practically all the other PI individuals. $A_{IUS}$ contributes with 3 lags ($A_{IUS}$(k-11), $A_{IUS}$(k-12) and $A_{IUS}$(k-14)) to the best individual input set, in addition it appears in 8 of the 9 PIs marking its importance in this temperature prediction environment. The central frequency of the component originated by the IUS transducer contributes with 2 lags ($F_{IUS}$(k-1) and $F_{IUS}$(k-6)), being present in 5 of the PIs. The dependence of the temperature on $BW_{IUS}$ is justified by the presence of $BW_{IUS}$(k-8). The relevance of TP is imposed by the presence of TP(k-4) and TP(k-13), in addition it information is present in 8 out of 9 PIs, marking it relevance. The past memory of the system is represented by the presence of T(k-10), T(k-15), and T(k-17).

Comparing the two best individuals input set it can be said that the number of inputs differs in one. The variable lags chosen are very different, existing only one coincident term (T(k-17)). Although, the measured temperature signals for the two distances considered have the same behaviour, i.e. the temperature tends to


ISSN: 1727-1983 © 2005 IFMBE

increase in the heating phase and to decrease in the cooling phase, the TUS beam pattern are different at the two distances and temperature increasing and decreasing differently, imposing a different input selection. In addition, genetic algorithms are based in an initial population randomly generated that is evaluated in a probabilistic schema based on the individual's performance, and the final PIs input sets are the ones that produce a good temperature prediction, being different between runs.

Looking at Table 3 it can be said that the best individual for the 24-mm experiment fulfils 4 out of 6 goals defined in the MOGA. The goals that were not fulfilled were the MC and the $R_{ue}$. Although the goal defined for $R_{ue}$ was not fulfilled, the value attained for this measure is close to the defined goal. Table 5 presents the MOGA optimisation objectives for the best individual at 48 mm. Looking at that Table it can be stated that this individual fulfils 5 out of 6 goals defined, the one that was not fulfilled is the MC. This goal was not fulfilled in both best individuals and in the majority of the PIs, indicating that for temperature prediction in the conditions used in this work good RBFNN must have MC≥100.

In Figures 4 and 6 the predicted and measured temperature waveforms, and the error in conjunction with it distributions are presented for the 24 and 48-mm experiment, respectively. From the figures it can be stated that in both experiments the prediction follows the measurement with a maximum absolute error less than 0.5 ºC, and a mean error close to 0 ºC. For the 24-mm experiment the error variance and bias is greater than for the 48-mm experiment. This can be explained by the fact that the point at 24 mm is within the beam near field while at 48 mm it is already the far field. At 48 mm the beam pattern is more regular, and less noisy features and temperature signals were obtained. In addition the results obtained are better or approximately equal to the ones obtained in the reference literature [2], for a larger prediction horizon and temperature range.

## Conclusions

These initial results suggest that the proposed type of non-linear black-box model performs well for discrete multi-point temperature prediction in homogeneous media (maximum absolute error less than 0.5 ºC). It opens the possibility of real-time monitoring of specific points on the tissue under therapy. The next step is to increment the model to multilayer inhomogeneous medium and try to build single models for multipoint temperature prediction.

## Acknowledgements

The authors would like to acknowledge the financial support of: Fundação para a Ciência e a Tecnologia (grant SFRH/BD/1461/2003), Portugal; and Conselho Nacional de Desenvolvimnto Científico e Tecnológico (CNPq/CYTED/490.013/03-1), Brazil. We also thank Eng. Hector Gomez and MSc. Guillermo Cortela for the help in the experimental setup.

## References

[1] ARTHUR R. M., STRAUBE W. L., STARMAN J. D., and MOROS E. G. (2003): 'Noninvasive Temperature Estimation Based on the Energy of Backscattered Ultrasound', *Medical Physics*, **30**, pp. 1021-1029.

[2] SIMON C., VANBAREN P., and EBBINI E.S. (1998): 'Two-dimensional Temperature Estimation Using Diagnostic Ultrasound', *IEEE Trans. on UFFC*, **45**, pp. 1088-1099.

[3] C. A. TEIXEIRA, G. CORTELA, H. GOMEZ, M. G. RUANO, A.E. RUANO, C. NEGREIRA, and W. C. A. PEREIRA (2004): 'Temperature Models of a Homogeneous Medium under Therapeutic Ultrasound', *IFMBE News*, **69**, pp. 52-56. Internet site address: http://ifmbe-news.iee.org/ifmbe-news/nov2004/nov04s.pdf.

[4] FONSECA C. M. and FLEMING P. J. (1993): 'Genetic algorithms for multi-objective optimisation: Formulation, discussion and generalization.', Proc. of 5th Int. Conf. Genetic Algorithms, pp. 416-423.

[5] FERREIRA P. M., RUANO A. E., and FONSECA C. M. (2003): 'Genetic Assisted Selection of RBF Model Structures for Greenhouse Inside Air Temperature Prediction', Proc. of IEEE Conf. on Control Applications, Istambul, Turkey, 2003, pp. 576-581.

[6] RUANO, A. E., FLEMING, P. J., and JONES, D. I. (1992): 'A connectionist approach to PID autotuning', *IEE Proceedings*, Brighton, UK, Part D, **139**, pp. 279-285.

[7] CHINRUNGRUENG, C. and SQUIN, C. H. (1995): 'Optimal adaptive K-means algorithm with dynamic adjustment of learning rate', *IEEE Trans. Neural Netw.*, **6**, pp. 157-169.

[8] BILLINGS S. and VOON W. (1986): 'Correlation Based Model Validity Tests for Nonlinear Models', *International Journal of Control*, **44**, pp. 235-244.


ISSN: 1727-1983 © 2005 IFMBE